15th International Symposium on Computer Methods in Biomechanics and Biomedical Engineering
and
3rd Conference on Imaging and Visualization
CMBBE 2018
P. R. Fernandes and J. M. Tavares (Editors)

Quantitative method for the three-dimensional assessment of human cortical long-bone architecture based on micro-CT images

Xavier Roothaer*, Remi Delille*, Herve Morvan*, Bruno Bennani*, Eric Markiewicz*, Christian Fontaine†

*Univ. Valenciennes, CNRS, UMR 8201 - LAMIH
F-59313 Valenciennes, France
xavier.roothaer@univ-valenciennes.fr

†Department of Anatomy, Faculty of Medicine, University of Lille 2
Place de Verdun - 59045 Lille cedex - France

Keywords: Biomechanics, Biomedical Engineering, Imaging, Computer Methods.

Abstract: The cortical bone is the part of bones which ensures the mechanical stiffness of the skeleton. To provide blood supply, numerous vascular canals pass through the bone matrix. This canal lattice has a preferred orientation and is interconnected. The aim of this study is to provide a method which is able to identify the 3D features of the canals network and its connectivity using μ-CT images in order to supply the cortical bone architectural data. An original algorithm, based on Python, is developed. It extracts the contours from the thresholded images and identifies 3D link between consecutive images in order to reconstruct the canals and computes the geometrical characteristics. Particular attention was paid to the threshold method by using an adaptive Otsu thresholding coupled with two image filters in order to reduce image noise. Furthermore, the algorithm is able to detect connectivity and thereby defines the beginning or the end of canals. Hence, each canal can be described with 14 characteristics. Likewise, some connectivity features are computed as the connectivity angle. Therefore, this study is the first one to propose an automated method for the connectivity detection and thus a clear definition of cortical canals which may quantify the cortical architecture of bone samples. In order to confirm the process, two close bone samples are studied. Results show small difference between samples which validate the current study.

1. Introduction

Long human bones are mostly divided in two distinct portions: a highly porous portion called trabecular bone located at each end of the bone (epiphyses), and a fewer porous portion called cortical bone located in the central part (diaphysis) which mainly provides the general stiffness of the bone. In spite of the mechanical functions, the cortical bone also has a highly connected porous architecture which ensures the blood vessel supply inside the bone. For several decades, it is widely admitted that a cellular activity, called BMU activity, which ensures the dynamic bone remodelling, is closely related to mechanical stimulus [1]. The BMU structure

can be interpreted as a 3D oriented canal which presents a closing cone on one side and connectivity on the other side [2]. Consequently, BMU activity is embedded in the cortical architecture and its analysis is necessary to quantify bone remodelling. This work aims at proposing a new method to quantify vascular porosity of cortical bone. Micro-tomographic device is employed. The python script extracts edges from slice images and then creates three-dimensional canals using centroids. Prior an image processing is applied to reduce impact of image quality on results. More than ten features are computed for each canal and connectivity. Finally, two femoral bone samples are extracted close to each other in order to suppose same architecture. Specimens are scanned and results are shown in Results and discussion section of this paper.

2. Material & methods

2.1 Sample preparation

Two femoral specimens were harvested from a 64 years old male cadaveric subject (1.68m, 76 kg). To ensure bone hydration, subject was embalmed using phenol, glycerine, methanol and distilled water solution. The two specimens were extracted approximately 4 mm below the middle of the diaphysis and along the longitudinal axis. The diaphysis was first sectioned using a surgical saw so as to reduce local heating. Then, sections were cut with a precision saw to obtain 60*10*1 mm rectangular parallelepiped samples aimed for mechanical testing (Figure 1). Each sample was extracted close to each other in order to obtain same architecture. Thus, results can be compared and validate the algorithm processing.

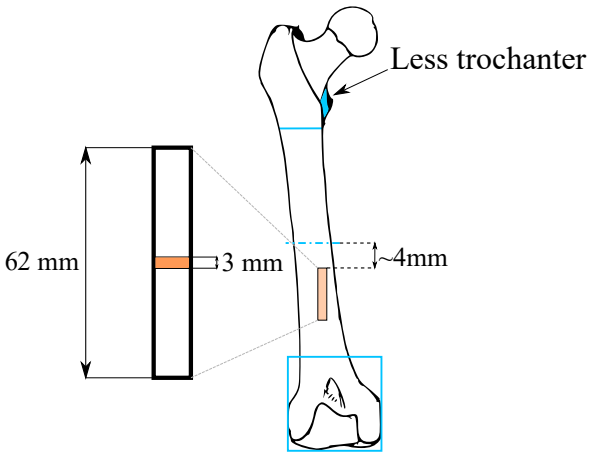

Figure 1. Extraction site of femoral samples.

2.2 Micro-Computed Tomography

SkyScan 1172 high resolution desktop micro-CT (80 kV, 100 μA, 0.25 degrees) was used. Each sample was scanned along the longitudinal axis with a 2.94 μm isotropic resolution. As shown by Figure 1, the scan was focused on a 3 mm region located in the middle of the sample. Hence, about 1,000 cross-sectional images were obtained.

2.3 Python script

2.3.1 Edge detection

This script is based on the edge detection on slice images. To reduce noise effects, care was taken to the threshold method. Indeed, rectangular shape of cross-section amplifies beam-hardening artefacts on CT images. Beam-hardening artefacts creates brightness gradient due to X-ray absorption. Consequently, bilateral and morphological filters are used with a sectioned Otsu threshold algorithm. Thus, each filtered image is portioned along the brightness gradient so as to apply local threshold. Then, edges are detected using OpenCV function (Figure 2) [3].

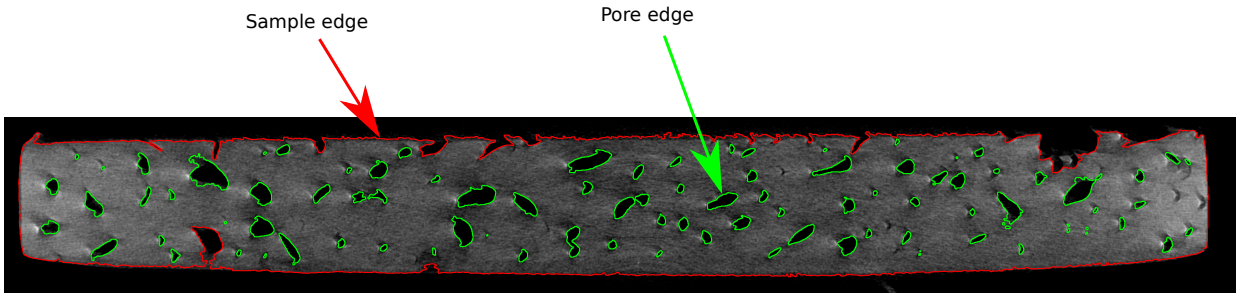

Figure 2. Image resulting from the image processing. Sample and pore edges are dissociated using their area value.

2.3.2 Three-dimensional creation of canals and connectivity detection

In order to create canals, centroids are computed for each pore. Hence, pores can be connected with another one located on a following slice. This connection occurs only if both centroids are located inside the same equivalent circle (Figure 3). Figure 3 is an illustrative example of 3D canals creation process. For instance, numbered pore 13 (from current image) is linked with numbered pore 12 (from downstream image) because they are both located inside the same equivalent circle.

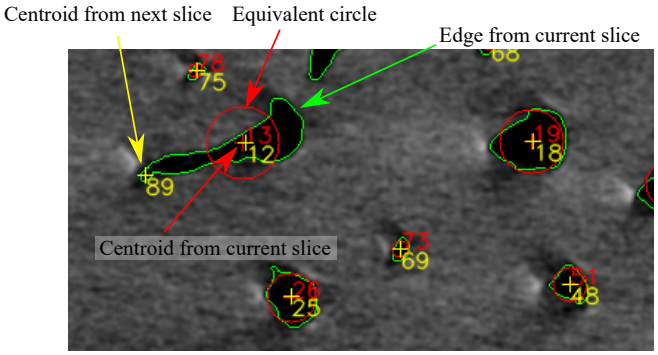

Figure 3. 3D canal creation. On this image, detected edges, centroids and equivalent circles are drawn in green and red, respectively. Centroids from downstream slice are drawn in yellow.

Connectivity detection is carried out after canal creation. Indeed, to ensure representative

data, canals are split on each connection. Connections are quantified if an extreme contour of a canal encloses the centroid from another canal.

2.3.3 Geometrical characteristics

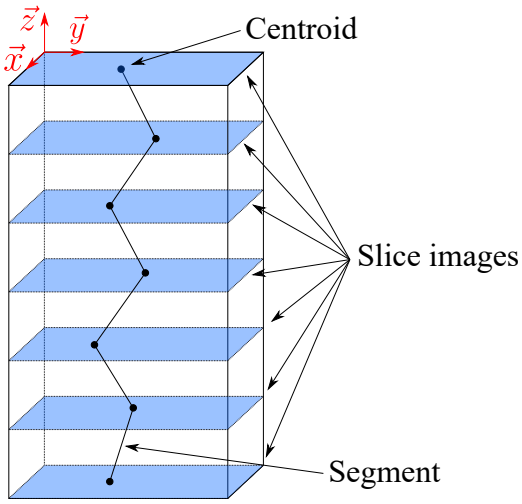

Figure 4. Canal is a set of segments which links centroids.

Several characteristics are computed for canals. Orientation is defined by two different angles : Φ and Θ. The first one defines the longitudinal orientation of canals using the angle between $\vec{z}$ axis and the canal segment. The second one represents the transverse orientation of canals using the angle between $\vec{x}$ axis and the canal segment (Figure 4). Thus, Φ ranges from 0 deg (longitudinal orientation) to 90 deg (transverse orientation) and Θ ranges from -90 deg to 90 deg (oriented along $\vec{y}$). Canal diameters are computed considering orientation of each segment. A 3D aspect ratio is processed so as to evaluate the tree-dimensional shape of canals. Indeed, if the ratio is below one, canal has a flat shape. Conversely, ratios over one means that the canal has an elongated shape. This ratio is computed according Equation 1.

$$\text{3D aspect ratio} = \frac{\text{Canal length}}{\text{Canal diameter}} \tag{1}$$

Some features are assessed for canal connections. For example, angle between connected canals is evaluated. Thus, tight connections have an angle close to zero, whereas wide connections have an angle up to 90 degrees. Canal and connectivity densities are computed using the ratio between the number of elements and the volume of the sample (usually called TV). Volume fraction of canals, usually called BV/TV, was computed for each sample. In order to validate this new method, BV/TV was computed using two different ways. The first one consists in computing BV/TV for each image and reporting the mean and standard deviation values. The second method computes BV/TV from the sum of canals volume fractions.

3. Results and discussion

The two samples were studied and results are stored in Table 1 for mean values and in Figure 5 for plot results.

	Φ $[deg]$	Θ $[deg]$	Canal length $[\mu m]$	Canal diameter $[\mu m]$	3D shape factor -	Connectivity angle $[deg]$
Sample 1	27.84 ± 14.20	-3.89 ± 40.15	151.41 ± 242.56	79.36 ± 74.07	2.86 ± 4.87	34.39 ± 21.49
Sample 2	26.73 ± 13.42	-0.42 ± 39.88	138.71 ± 205.80	80.02 ± 77.34	2.18 ± 2.83	29.54 ± 20.00

Table 1. Statistical results of canals and connectivity characteristics. Mean $\pm$ standard deviation is shown.

The comparison between 2D and 3D BV/TV reveals a small difference between these two values. Indeed, the 2D BV/TV for the first specimen equals to 7.22% (± 0.69) and 3D BV/TV equals to 7.00%. This difference is justified by residual noises and edge effects which are not considered as canals. Consequently, they are not considered in 3D BV/TV (computed from canals). Interestingly, the second sample shows similar differences (2D BV/TV = $7.22 \pm 0.61\%$, 3D BV/TV = 7.03%). Furthermore, the cortical porosity is in accordance with Cooper et al. study [4]. The orientation of canals reveals a canal network which is oriented along an oblique axis of about 25 degrees (Figure 5a) and randomly arranged in cross-section plane (Figure 5b).

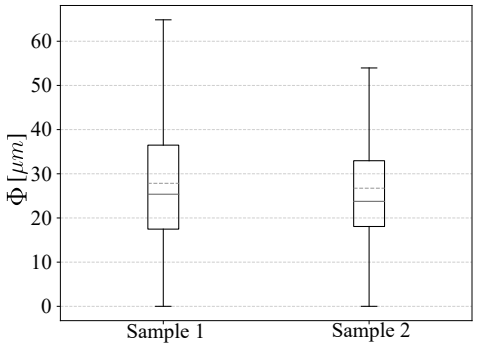

(a) Boxplot of Φ angle

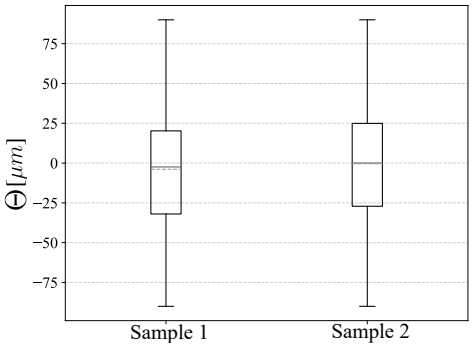

(b) Boxplot of Θ angle

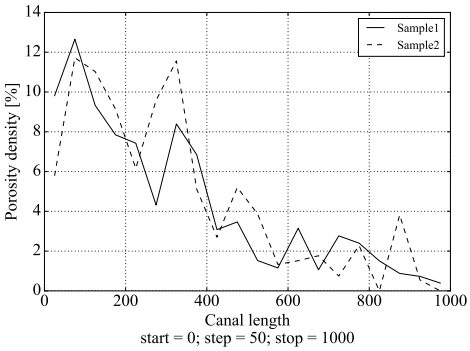

(c) Porosity density for canal length

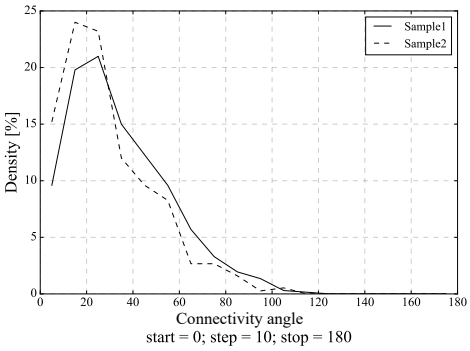

(d) Histogram of connectivity angle

Figure 5. Statistical results of canals and connectivity geometry

The statistical distribution of canal characteristics are the same for the two samples (Table 1). Large standard deviation proves that canal features are not normally distributed. 50% of the porosity is induced by canals with a length over 260 μm (Figure 5c). A study highlighted longer canals but without separating on connections [2].

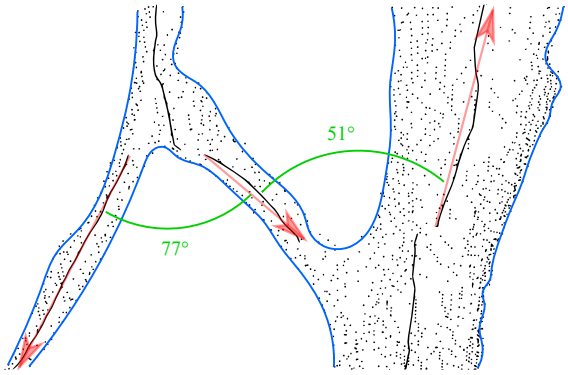

Figure 6. Vector graphic obtained from a snapshot of a 3D view of canals and centroids wire line. Computed connection angles are highlighted. Red arrow is the linear fitting of centroids line.

Figure 5d reveals that canals are mostly connected with an angle of 30 degrees. Figure 6 shows a snapshot of 3D scatter point of a typical cortical connectivity. In accordance with the canal definition, canals are separated at each connection. No significant correlation was found between characteristics.

4. Conclusion

This study aimed at proposing a new method to accurately describe cortical architecture using tomographic slices. The python algorithm is based on edge detection. An optimised image processing is used in order to reduce the influence of global thresholding on results. In order to validate the script processing, two bone samples were harvested from the same location in the femoral diaphysis of a male subject. Results are quite revealing in several ways. First, in spite of the influence of image quality, statistics for the two specimens are similar. This validates the image processing and computation canal characteristics. Second, the orientation reveals that the canal network is not purely longitudinal. For this reason, the orientation should be considered for the correlation with mechanical tests. In future investigations, it might be possible to use this script so as to correlate architecture parameters with age, morphology, gender of human subjects.

References

[1] H. M. Frost. Tetracycline-based histological analysis of bone remodeling. *Calcified Tissue Research*, 3(3):211–237, 1969.

[2] D.M.L. Cooper, A.L. Turinsky, C.W. Sensen, and B. HallgrÃmsson. Quantitative 3d analysis of the canal network in cortical bone by micro-computed tomography. *The Anatomical Record Part B: The New Anatomist*, 274B(1):169–179, September 2003.

[3] Gary R. Bradski and Adrian Kaehler. *Learning OpenCV: computer vision with the OpenCV library*. Software that sees. O'Reilly, Beijing, 1. ed., [nachdr.] edition, 2011. OCLC: 838472784.

[4] David M. L. Cooper, C. David L. Thomas, John G. Clement, Andrei L. Turinsky, Christoph W. Sensen, and Benedikt HallgrÃmsson. Age-dependent change in the 3d structure of cortical porosity at the human femoral midshaft. *Bone*, 40(4):957–965, April 2007.